[1]D. R. Bates, *Atomic and Molecular Processes* (Academic, New York, 1962), pp. 597–621.
[2]E. E. Nitikin, J. Chem. Phys. **43,** 744 (1965).
[3]E. E. Nitikin, Comments At. Phys. **2,** 122 (1970).
[4]R. H. G. Reid and A. Dalgarno, Phys. Rev. Lett. **22,** 1209 (1969).
[5]R. H. G. Reid and A. Dalgarno, Chem. Phys. Lett. **6,** 85 (1970).
[6]D. C. S. Allison and P. G. Burke, J. Phys. B **2,** 941 (1969).
[7]Correct to within terms of order $m_e/(m_A+m_B)$. See M. H. Mittleman, Phys. Rev. **188,** 221 (1969).
[8]R. T. Pack and J. O. Hirschfelder, J. Chem. Phys. **49,** 4009 (1968).
[9]F. T. Smith, Phys. Rev. **179,** 111 (1969).
[10]W. R. Thorson, J. Chem. Phys. **34,** 1744 (1961).
[11]A. C. Wahl, P. Julienne, and M. Krauss, Chem. Phys. Lett. **11,** 16 (1971).
[12]P. Julienne, M. Krauss, and D. Neumann, 1971 (unpublished).
[13]We also shall have use of the property that they are eigenfunctions of the parity (inversion)operator $g|(n, L, S)m_L, m_S\rangle (-1)^L|(n., L, S)m_L, m_S\rangle$.
[14]This limiting behavior is only true for finite values of r_i. It is possible for one of the electrons, e.g., $i=k$, to transfer to the proton such that $|\vec{r}_k-\vec{R}|$ remains finite as $R\to\infty$, in which case H_{AB} asymptotically consists of the F^+ and H atomic Hamiltonians, rather than $F+H^+$. This is the charge transfer, or rearrangement channel, and molecular states exist which asymptotically correlate with this channel. At high energies (threshold $E=3.825$ eV) such molecular states must be included, but at the low energies considered here they yield closed scattering channels and will be ignored. It should be noted that such atomic charge-transfer states do contribute to the molecular states at finite R, even for the $F+H^+$ channel, and hence the molecular theory does include "adiabatic" coupling to the closed charge-transfer channel.
[15]T. E. H. Walker and W. G. Richards, Symp. Faraday Soc. 64 (1968).
[16]T. E. H. Walker and W. G. Richards, Phys. Rev. **177,** 100 (1969).
[17]M. E. Rose, *Elementary Theory of Angular Momentum* (Wiley, New York, 1957).
[18]$\mathcal{E}_\alpha$ may be an implicit function of R, $\mathcal{E}_\alpha(R)$, which approaches a constant as $R\to\infty$.
[19]In the theory of molecular spectra $\vec{L}_R^2$ is often designated as $\vec{N}^2$ or $\vec{R}^2$ with eigenvalues $N(N+1)$ or $R(R+1)$.
[20]G. Herzberg, *Spectra of Diatomic Molecules* (Van Nostrand, Princeton, N. J., 1950).
[21]R. S. Mulliken, Rev. Mod. Phys. **4,** 24 (1932).
[22]$\mathcal{G}_{l,l',M}\equiv\langle l, j, m_l, m_j|T|l', j', m_l', m_j'\rangle\,\delta_{m_l,\,M-m_j}\,\delta_{m_{l'},\,M-m_{j'}}$ where $\langle T\rangle$ is the transition matrix element for channel states represented as $|l, j, m_l, m_j\rangle\equiv Y_{l,m_l}(\theta,\phi)|\vec{R}, j, m_j\rangle$. These have been combined in (5.6) to produce the total angular moment states $|R, J, M, j, l\rangle$.
[23]G. Grawert, Z. Phys. **225,** 283 (1969).
[24]F. P. Billingsley, II and M. Krauss, Phys. Rev. A **6,** 855 (1972).
[25]The parameters in (8.7) agree to within 10% with the more accurate values of F. P. Billingsley, II and W. Stevens who have studied the quadrupole constants and polarizabilities of the first-row atoms using the same techniques.
[26]J. H. Van Vleck, Rev. Mod. Phys. **23,** 213 (1951).
[27]W. Kolos and L. Wolniewicz, Rev. Mod. Phys. **35,** 473 (1963).

PHYSICAL REVIEW A VOLUME 7, NUMBER 3 MARCH 1973

Molecular Theory of Atomic Collisions: Calculated Cross Sections for $H^+ + F(^2P)$

F. H. Mies
National Bureau of Standards, Washington, D. C. 20234
(Received 11 September 1972)

The results of a close-coupling calculation of the fine-structure transitions $(j, m_j \to j', m_j')$ are presented for collisions between photons and $F(^2P_{j,m_j})$. The theory is formulated in the perturbed-stationary-state approximation using accurate molecular wave functions for the ground $^2\Pi$ and $^2\Sigma$ states of HF^+. Comparison is made to the predictions of the Born approximation. The magnetic selection rule $(j, m_j \to j, -m_j)$ is strongly violated in the $j=3/2$ state and less strongly violated in the $j=1/2$ state. It is concluded that the important region of interaction for the $j=1/2 \to j=3/2$ transition is at short-to-intermediate distances where accurate molecular potentials are required and close-coupling effects are dominant.

I. INTRODUCTION

In the preceding paper[1] the theory of fine-structure transitions in proton-fluorine collisions was developed using the ground molecular $HF^+(^2\Pi)$ and $HF^+(^2\Sigma)$ electronic states in a perturbed-stationary-state expansion of the scattering wave functions. At each total energy E, and for each total angular momentum state J, with space projection M, there exists a set of six open *molecular* channel states $|R, J, M, j, l\rangle$ arising from the six substates (j, m_j) of the $F(^2P_{j,m_j})$ ground state. The channel-state expansion (I-6.1) defines the radial functions $F^{J,M;E}_{j,l;j',l'}(R)$ which must vanish at $R=0$, and are subject to the asymptotic boundary conditions in Eq. (I-6.3) which determines the reactance matrix $K^J_{j,l;j',l'}$ and hence, the scattering cross sections. This expansion results in the coupled differential equations of Eq. (I-7.1) which may be written in the following matrix form:

$$\left[\left(-\frac{\partial^2 R}{2\mu R\partial R^2}-E\right)\underline{1}+\underline{U}^J(R)\right]\underline{F}^{J,M,E}(R)=0\,, \quad (1.1)$$

where

$$\underline{F}^{J,M,E}=\{F^{J,M;E}_{j,l;j',l'}\}$$

and

$$\underline{1}=\{\delta_{j,j'}\delta_{l,l'}\}\,.$$

The interaction matrix $\underline{U}^J(R)$ is obtained from Eqs. (I-7.2) and (I-7.3), utilizing the result that the Born-Oppenheimer (BO) terms (I-7.2b) and (I-7.2c) are negligible for HF^+,

$$U^J_{j,l;j',l'}(R) = \delta_{j,j'}\delta_{l,l'}\left(\mathcal{E}_j + W_1(R) + \frac{l(l+1)}{2\mu R^2}\right) + C^J_{j,l;j',l'}[W_0(R) - W_1(R)], \quad (1.2)$$

where the J-dependent coefficients $\underline{C}^J$ are defined in Table I-2. $W_1(R)$ is the $^2\Pi$ and $W_0(R)$ is the $^2\Sigma$ molecular potential, as shown in Figs. I-2 and I-3, and both exhibit the R^{-3} asymptotic dependence summarized in Eq. (I-8.7). The interaction coefficients $\underline{C}^J$ are partially diagonalized owing to parity conservation, and the application of the theory reduces to solving two sets of three coupled differential equations of the form (1.1) for each J. One set yields the radial functions for the channel states $j=\frac{3}{2}$, $l=J+\frac{3}{2}$, $J-\frac{1}{2}$ and $j=\frac{1}{2}$, $l=J-\frac{1}{2}$, with parity $(-1)^{J+1/2}$; and the other set yields solutions for states $j=\frac{3}{2}$, $l=J-\frac{3}{2}$, $J+\frac{1}{2}$, and $j=\frac{1}{2}$, $l=J+\frac{1}{2}$ of opposite parity $(-1)^{J-1/2}$. The six resultant regular solutions define $\underline{K}^J$ and the transition matrix $\underline{T}^J$ which is combined and summed over J, l, l' in Eqs. (I-6.10)–(I-6.19) to yield the appropriate cross sections. This paper will be concerned with the solution of these equations and the calculation of the total cross sections over the energy range from threshold to $E \approx 0.25$ eV.

In Sec. II, the numerical procedures that are used are outlined, and some intermediate results which demonstrate the utility and accuracy of the methods are presented. The cross sections are presented in Sec. III, and the results are discussed in Sec. IV. Section V contains a comparison between the exact results and the two-state Born approximation. Finally, the general conclusions are summarized in Sec. VI.

II. NUMERICAL PROCEDURE AND ACCURACY OF CLOSE-COUPLING CALCULATIONS

Equation (1.1) may be simplified with the substitution,

$$\underline{G}^{J,M,E}(R) = R\underline{F}^{J,M,E}(R) \quad (2.1)$$

such that

$$\left[\left(\frac{\partial^2}{2\mu\,\partial R^2} + E\right)\underline{1} - \underline{U}(R)\right]\underline{G}(R) = 0\,. \quad (2.2)$$

The superscripts J, M, E, which are constants will be suppressed and left implicit. Obviously, since $\underline{U}^J \neq \underline{U}^J(M)$, the radial functions are actually independent of M; the entire M dependence of the total wave function $\Psi(J, M, E)$ in Eq. (I-6.1) is embodied in the channel-state functions.

Equation (2.2) is solved numerically using the Gordan algorithm.[2,3] The method is thoroughly outlined in Gordan's lucid papers, and only very minor variations have been introduced. The major difference comes in the use of trigonometric functions rather than Airy functions as the reference solutions. That is, the symmetric matrix $\underline{U}(R_0)$ evaluated at the midpoint $R_0 = \frac{1}{2}(R_L + R_R)$ of each integration interval $R_L \leqq R \leqq R_R$ is diagonalized:

$$\underline{U}(R_0) = \tilde{\underline{M}}\,\underline{V}^0\,\underline{M}\,, \quad (2.3)$$

and the independent sets of trigonometric functions $\underline{A}(R)$, $\underline{B}(R)$ which are solutions of the uncoupled equations

$$\left[\left(\frac{\partial^2}{2\mu\,\partial R^2} + E\right)\underline{1} - \underline{V}^0\right]\begin{Bmatrix}\underline{A}(R)\\ \underline{B}(R)\end{Bmatrix} = 0 \quad (2.4)$$

are used as a basis to expand the exact solutions.

$$\underline{G} = \tilde{\underline{M}}[\underline{A}\,\underline{a} + \underline{B}\,\underline{b}]\,, \quad \underline{G}' = \tilde{\underline{M}}[\underline{A}'\underline{a} + \underline{B}'\underline{b}]\,. \quad (2.5)$$

Coupled first-order equations are developed for $\underline{a}(R)$ and $\underline{b}(R)$ with boundary conditions at $R = R_L$ determined by the given values of $\underline{G}(R_L)$ and $\underline{G}'(R_L)$. The equations for $\underline{a}$ and $\underline{b}$ are integrated to $R = R_R$ and used in Eq. (2.5) to determine $\underline{G}(R_R)$ and $\underline{G}'(R_R)$. This procedure is repeated and carried out to some predetermined distance R_{max} at which the calculated wave functions $\underline{G}(R_{max})$ and $\underline{G}'(R_{max})$ are used to evaluate the reactance matrix $\underline{K}^J$ according to the boundary conditions set in Eq. (I-6.3). A subroutine is used to generate the required spherical Bessel functions $j_l(k_j R_{max})$ and $n_l(k_j R_{max})$ with an accuracy of 10^{-7} or greater.

The over-all philosophy in generating the program was to sacrifice speed for accuracy and precision. It is difficult to carry out an analysis of the errors propagated by the integration techniques (see Gordan[3]) but all the criteria employed in choosing step sizes and evaluating integrals, etc., have been extremely conservative. Four features of the program and its accuracy are outlined below.

(i) The leading asymptotic term in Eq. (1.2) is, of course, the $l(l+1)/2\mu R^2$ centrifugal term, which, in the absence of $W_0(R)$ and $W_1(R)$ would simply generate the regular spherical Bessel function $j_l(k_j R)$, with the result that the $\underline{K}^J$ matrix, which is a measure of the irregular component $n_l(k_j R)$, should vanish. Since the cross sections must be summed to values of $l \leqq 300$, the program's ability to reproduce the Bessel function solutions when $W_0 = W_1 = 0$ was tested. The calculated $\underline{K}$ matrix for l values up to 300, and for k_j values of the required range, is of the order 10^{-6} or less for the integration parameters employed in the subsequent calculations. This suggests that at least the diagonal $\underline{K}$ matrix elements generated in the presence of the interaction potentials are also of this accuracy.

(ii) Each column vector in $\underline{G}$ is an independent solution and is generated by *choosing* initial values of $\underline{G}(R_{int})$ and $\underline{G}'(R_{int})$ at some initial point $R = R_{int}$

such that the vectors are linearly independent and satisfy the inner boundary condition that $\underline{G}(R)\sim 0$ as $R\to 0$. The solutions were initialized by setting $\underline{G}(R_{\rm int})=0$ and $\underline{G}'(R_{\rm int})=\underline{1}$, and choosing $R_{\rm int}$ such that

$$|G(R_{\rm max})|+|G'(R_{\rm max})|\geq 10^{12}. \tag{2.6}$$

The final results are entirely insensitive to the choice $R_{\rm int}$ as long as (2.6) is satisfied. However, they are sensitive to the initial choice of step size $h=R_R-R_L$, unless this initial value is reduced below about 10^{-2} a.u. A more clever choice would have been to set $\underline{G}(R_{\rm int})=\underline{\tilde{M}}(\underline{V}^0-E)^{-1/2}\underline{M}$, and $\underline{G}'(R_{\rm int})=1$. However, if the integration is begun sufficiently close to the origin, then $\underline{V}^0\sim\infty$ and $\underline{G}\sim 0$ and the initial guess $\underline{G}=0$ should be valid. In any case, after the first few integration steps the solutions settled down to a very stable independent set of vectors which are insensitive to wide variations in the initial conditions, $R_{\rm int}$, and h.

(iii) The integration was carried out to $R_{\rm max}\geq$ Max $\times(l^2/k_j,\ 1000)$ and generally $R_{\rm max}\approx 5-10\times 10^3$ a.u. The resultant $\underline{K}^J$ matrix is insensitive to this choice to 10^{-6} or less as long as accurate Bessel function programs are used in the fitting. A maximum integration step size $h_{\rm max}$ of 500 a.u. was used which allowed rapid integration to these large distances. Variation of $1\leq h_{\rm max}\leq$ unlimited produced negligible changes indicating that $\underline{a}(R)$ and $\underline{b}(R)$ in Eq. (2.5) are very insensitive functions of R at large distances and are well calculated by the integration techniques used in the program.

Additional confidence in the numerical results is obtained from the symmetry of the calculated $\underline{K}$ matrix. Note that $K_{i,j}=K_{j,i}$ to within one part in 10^4 even for $K_{i,j}=O(10^{-4})$ and they are generally symmetric to within one part in 10^5–10^6 for larger elements.

(iv) The program was tested against the results of Lester[4] for a variety of three-coupled-state calculations in He + H_2 rotational excitation, and the calculated $S_{i,j}$ matrix elements agreed to $1/10^4$ or better down to $|\underline{S}|=O(10^{-3})$.

III. EVALUATION AND PRESENTATION OF CROSS SECTIONS

At each energy E the reactance matrix $K^J_{j,l;j',l'}$ was determined as a function of J. This matrix defines the transition matrix $\underline{T}^J=-2i\underline{K}^J(\underline{1}-i\underline{K}^J)^{-1}$ which is used in the evaluation of the total cross sections

$$\bar{\sigma}_{j,m_j\to j',m_j'}=\sum_{l,l',M}\left(\frac{\pi}{k_j^2}\right)\mathcal{S}_{l,l',M}\,\mathcal{S}^*_{l',l',M} \tag{3.1}$$

and

$$\sigma^0_{j,m_j\to j',m_j'}=\sum_{l,l',l''} i^{l-l''}\left(\frac{\pi}{k_j^2}\right)(2l+1)^{1/2}(2l''+1)^{1/2}$$
$$\times\mathcal{S}_{l,l',m_j}\,\mathcal{S}^*_{l'',l',m_j}, \tag{3.2}$$

where[5]

$$\mathcal{S}_{l,l',M}=\sum_J(l,\ j,\ J\,|\,M-m_j,\ m_j,\ M)$$
$$\times(l',\ j',\ J\,|\,M-m_j',\ m_j',\ M)\,T^J_{j,l;j',l'}$$
$$\equiv\langle j,\ m_j,\ l,\ m_l\,|\,T\,|\,j',\ m_j',\ l',\ m_l'\rangle$$
$$\times\delta_{M,m_j+m_l}\delta_{M,m_j'+m_l'}. \tag{3.3}$$

The calculated cross sections for $E=0.002$ a.u. are presented in Table I. An effective temperature can be defined by equating kT to the incident kinetic energy $\epsilon=(E-\mathcal{E}_j)$, where $\mathcal{E}_{1/2}=a$, $\mathcal{E}_{3/2}=-\frac{1}{2}a$ and $a=0.001228$ a.u. for $F(^2P)$. Thus, the tabulated cross sections pertain to effective temperatures of ~250 and ~800 °K for collisions in incident channels $j=\frac{1}{2}$ and $j=\frac{3}{2}$, respectively. The series are explicitly summed to $l=125$. The contributions (< 10%) from $l=126$ to ∞ are accurately determined by techniques discussed below.

The isotropic cross sections $\bar{\sigma}$ in Table I(a) are the total cross sections for the transition $j,\ m_j\to j',\ m_j'$ averaged over a random isotropic distribution of incident wave vectors $\hat{k}_j$. This cross section is directly related to the gas-phase rate constants for the fine-structure transitions, and the numerical results exhibit the detailed balance, i.e., $k_j^2\bar{\sigma}_{j,m_j\to j',m_j'}=k_{j'}^2\bar{\sigma}_{j',m_j'\to j,m_j}$, that is required by Eq. (3.1), and the precepts of statistical mechanics. An alternate expression [Eq. (I-6.19)] derived from irreducible tensors leads to identical results indicating that the summations in Eq. (3.1) were properly (and wastefully) handled.

The zero-angle cross section σ^0 tabulated in Table I(b) is a specialized total cross section possibly pertinent to a beam experiment where the incident plane wave propagates along the axis of quantization of the target atomic states. This is the total cross section normally presented in standard text books on scattering theory. It has long been recognized that for this total cross section transitions between degenerate magnetic sublevels (j, $m_j\to j,\ m_j'$) do not of necessity obey detailed balance, as can be seen in Table I(b). However the isotropic cross section $\bar{\sigma}$, averaged over all incident wave vectors, *including* the specialized $\hat{k}_j=0$ case, does yield the necessary balance, as well it must. It is apparent on comparing Tables I(a) and I(b) that measurements of magnetic sublevel transitions in a beam experiment, which selects a given incident wave vector, can lead to highly deceptive conclusions concerning the gas-phase rate constants. This is a general phenomenon with spatially degenerate states. Note that both cross sections yield identical results, given in Table I(c), when they are summed and averaged over final and initial

TABLE I. Total cross sections at $E = 0.002$ a.u.

j, m_j	j', m_j' $\frac{3}{2}, \frac{3}{2}$	$\frac{3}{2}, \frac{1}{2}$	$\frac{3}{2}, -\frac{1}{2}$	$\frac{3}{2}, -\frac{3}{2}$	$\frac{1}{2}, \frac{1}{2}$	$\frac{1}{2}, -\frac{1}{2}$
(a) Isotropic total cross-sections $\bar{\sigma}_{j,mj\to j',mj'}$ (a_0^2)						
$\bar{\sigma}_{j,mj\to j',mj'}$ (a_0^2)						
$\frac{3}{2}, \frac{3}{2}$	1021.0	359.0	346.0	187.3	0.00551	0.01286
$\frac{3}{2}, \frac{1}{2}$		1003.5	204.7	346.0	0.00796	0.01041
$\frac{3}{2}, -\frac{1}{2}$			1003.5	359.0	0.01041	0.00796
$\frac{3}{2}, -\frac{3}{2}$				1021.0	0.01286	0.00551
$\frac{1}{2}, \frac{1}{2}$	0.0187	0.0269	0.0352	0.0435	1991.3	32.7
$\frac{1}{2}, -\frac{1}{2}$	0.0435	0.0352	0.0269	0.0187	32.7	1991.3
(b) Zero-angle total cross sections $\sigma^0_{j,mj\to j,mj'}$ (a_0^2)						
$\frac{3}{2}, \frac{3}{2}$	845.6	90.5	594.5	444.2	0.00068	0.00075
$\frac{3}{2}, \frac{1}{2}$	100.4	784.2	383.9	582.3	0.01395	0.02136
$\frac{3}{2}, -\frac{1}{2}$	582.3	383.9	784.2	100.4	0.02136	0.01395
$\frac{3}{2}, -\frac{3}{2}$	444.2	594.5	90.5	845.6	0.00075	0.00068
$\frac{1}{2}, \frac{1}{2}$	0.0275	0.0291	0.0338	0.0339	1975.0	49.0
$\frac{1}{2}, -\frac{1}{2}$	0.0335	0.0338	0.0291	0.0275	49.0	1975.0

(c) $\bar{\sigma}_{j,j'}$ Summed over m_j and averaged over m_j

	$j' = \frac{3}{2}$	$j' = \frac{1}{2}$
$j = \frac{3}{2}$	1913.0	0.01837
$j = \frac{1}{2}$	0.12436	2024.0

magnetic sublevels. This numerical result is also an additional check on our manipulation of the scattering matrices, etc., in constructing the cross sections.

The convergence of the partial-wave summations in Eq. (3.1) and (3.2) is demonstrated in the following graphs. The quantity

$$\sum_{l',M} \mathcal{G}_{l,l',M}\, \mathcal{G}^*_{l,l',M}$$

is plotted versus the partial-wave quantum number l in Fig. 1. The dashed line in the upper graph of Fig. 1 represents the upper bound that this summation can achieve, i.e., $4(2l+1)$, when $\underline{T} \to 2\times\underline{1}$. At large l the T matrix rapidly approaches small quantities which, as we shall see, are in quantitative agreement with the Born approximation. This is substantiated by the l^{-3} and l^{-5} dependence of the large-l contributions which are consistent with the R^{-3} and R^{-4} long-range potentials expected in the $j = \frac{3}{2}$ and $j = \frac{1}{2}$ channels, respectively. The l^{-7} dependence of the $\bar{\sigma}_l(\frac{3}{2}, \frac{3}{2} \to \frac{3}{2}, -\frac{3}{2})$ cross section is explicable in terms of a second Born approximation. Given the large-l dependence of the cross sections to be l^{-N}, the contribution of the infinite series may be approximated as follows:

$$\sigma \approx \sum_{l=0}^{l^*} \sigma_l + \sigma_{l^*+1}(l^*+1)/(N-1). \tag{3.4}$$

The partial-wave contributions to σ^0 also give the large-l dependence predicted by the Born approximation. These dependences for the specific magnetic transitions are summarized in Table II, and all the presented data have been adjusted according to formula (3.4).

IV. DISCUSSION OF RESULTS

A. Behavior of Cross Sections at a Specific Energy

Table I tabulates cross sections for $E = 0.002$ a.u. which roughly corresponds to a room-temperature collision. The $j = \frac{1}{2} \to j = \frac{3}{2}$ cross section in Table I(c) is of the order of $0.1a_0^2$. Although this is quite small, it is 10^2–10^3 times larger than the observed cross sections for, say, He + Cs, Rb collisions, which have comparable fine-structure splittings in the ^2P state. However, in F(^2P) the j states are inverted and the entire interaction potential behavior will be qualitatively different and such a comparison does not lead to any particular insight. On the other hand, the large size of the magnetic transitions, and elastic cross sections in Tables I(a) and I(b) are expected owing to the long-

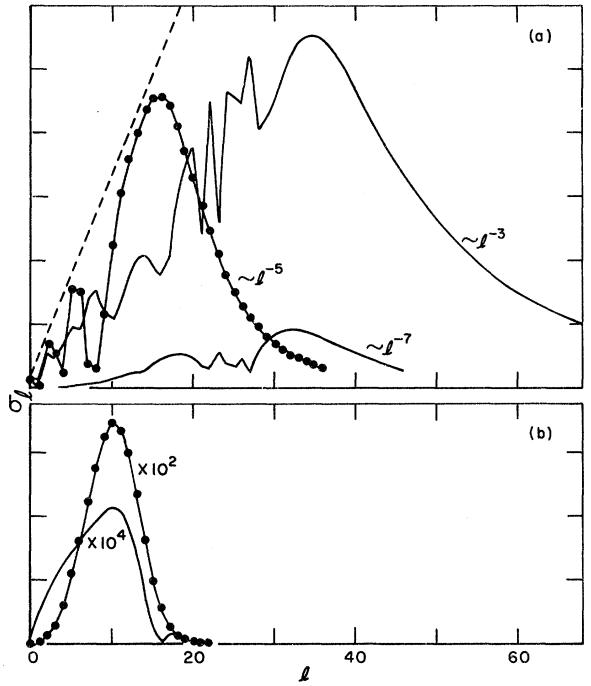

FIG. 1. Contribution of individual partial waves to isotropic total cross sections $\bar{\sigma}_{j,m_j\to j',m_j'}$. (a) The dashed linear curve represents the upper bound when $\underline{T}=\underline{2}$. The larger solid curve is the total cross reaction in the $j=\frac{3}{2}$ state, summed over all m_j. The smaller solid curve shows the substantial contribution ($\sim 10\%$) the "forbidden" $m_j=\frac{3}{2}\to-\frac{3}{2}$ transition makes to the total $j=\frac{3}{2}$ cross section. The dotted curve is for $j=\frac{1}{2}$ summed over m_j. (b) These cross sections are plotted on the same relative scale as (a) and have been magnified by 10^2 and 10^4. The solid curve is the total cross section for the $j=\frac{1}{2}\to j=\frac{3}{2}$ transition. The dotted curve is the magnetic $m_j=\frac{1}{2}\to-\frac{1}{2}$ transition in the $j=\frac{1}{2}$ state.

range ion-quadrupole interaction. What is "unexpected" is the magnitude of the $m_j=\frac{3}{2}\to-\frac{3}{2}$ cross section in the $j=\frac{3}{2}$ state, and the $m_j=\frac{1}{2}\to-\frac{1}{2}$ cross section in both $j=\frac{3}{2}$ and $\frac{1}{2}$. Various "selection rules" have been devised for these Zeeman transitions based on two-state perturbation theory and the Born approximation which predict that these cross sections should be zero. It is difficult to generalize, but it would appear doubtful that these so-called selection rules *ever* carry much validity, particularly for the $j=\frac{3}{2}$ state. The $m_j=\frac{1}{2}\to-\frac{1}{2}$ transition in the $j=\frac{1}{2}$ state is forbidden on more stringent grounds since it can only occur via intermediate coupling to the $j=\frac{3}{2}$ state, and a close correlation is expected between the inelastic $j=\frac{1}{2}\to\frac{3}{2}$ cross section and this magnetic transition. Yet even here, the cross section is rather large ($30a_0^2$) and some 200 times larger than the inelastic cross section.

This behavior is shown more explicitly in Fig. 1 where the contribution of each partial wave to the cross section is plotted versus l. Compare the two curves in Fig. 1(b); the solid curve is for the inelastic $j=\frac{3}{2}\to\frac{1}{2}$ transition, while the dotted curve is for the $m_j=\frac{1}{2}\to-\frac{1}{2}$ transition in $j=\frac{1}{2}$. Although it is 100 times larger, the latter transition only has contributions in the region of strong coupling[6] and parallels the inelastic cross section. Note particualrly that these two transitions peak at $l\approx 10$, and are negligible by $l\approx 20$. Since l is a measure of the classical impact parameter, we conclude that these cross sections are determined at small to intermediate distances. An l value of 10 would correspond to a critical distance of $R\approx 3$–10 a.u. In addition the cross section is determined in the region of strong coupling[6] where perturbation and two-state theories will fail. In terms of the molecular theory this means that the interaction potentials must be determined at short to intermediate distances where the asymptotic expansion of the potentials is invalid. Also accurate knowledge of the R dependence of the coupling matrix elements must be had, and one cannot generally rely on approximations such as neglecting the R dependence of the spin-orbit interaction. Such considerations should apply to most systems, except, *possibly*, to very light atoms where the spin-orbit splittings are quite small and the critical region of interaction is probably at large, asymptotically valid, R distances. A calculation of He + Na(^2P) scattering will be performed to assess the range over which accurate molecular potentials are required.

The top-most solid curve in Fig. 1(a) is for the total cross section in the $j=\frac{3}{2}$ state, while the low-

TABLE II. Large-l dependence of partial cross sections σ_l.

Transition	$\bar{\sigma}_l\sim \bar{C}l^{-N}$	$\sigma_l^0\sim C^0 l^{-N}$
$\frac{3}{2},\ \frac{3}{2}\to\frac{3}{2},\ \frac{3}{2}$	$N=3$	$N=5$
$\frac{3}{2},\ \frac{3}{2}\to\frac{3}{2},\ \frac{1}{2}$	3	7
$\frac{3}{2},\ \frac{3}{2}\to\frac{3}{2},\ -\frac{1}{2}$	3	3
$\frac{3}{2},\ \frac{3}{2}\to\frac{3}{2},\ -\frac{3}{2}$	7	7
$\frac{3}{2},\ \frac{1}{2}\to\frac{3}{2},\ \frac{1}{2}$	3	5
$\frac{3}{2},\ \frac{1}{2}\to\frac{3}{2},\ -\frac{1}{2}$	7	7
$\frac{3}{2},\ \frac{1}{2}\to\frac{3}{2},\ -\frac{3}{2}$	3	3
$\frac{3}{2},\ -\frac{1}{2}\to\frac{3}{2},\ -\frac{1}{2}$	3	3
$\frac{3}{2},\ -\frac{1}{2}\to\frac{3}{2},\ -\frac{3}{2}$	3	7
$\frac{3}{2},\ \frac{3}{2}\to\frac{3}{2},\ \frac{3}{2}$	3	5
$\frac{1}{2},\ \frac{1}{2}\to\frac{1}{2},\ \frac{1}{2}$	5	5
$\frac{1}{2},\ \frac{1}{2}\to\frac{1}{2},\ -\frac{1}{2}$	negligible contributions	
$\frac{1}{2},\ -\frac{1}{2}\to\frac{1}{2},\ -\frac{1}{2}$	5	5
$\frac{3}{2},\ m_j\to\frac{1}{2},\ m_j'$	negligible contributions	

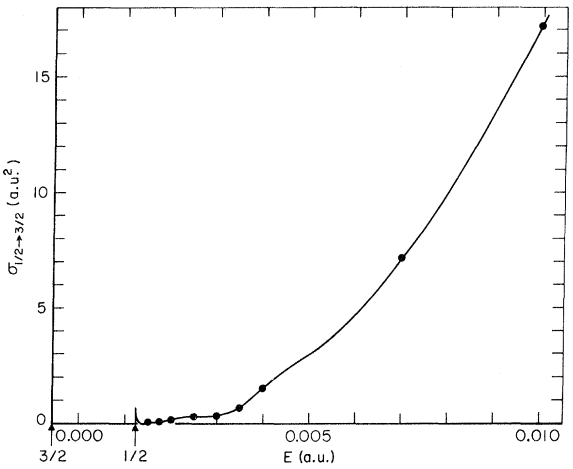

FIG. 2. Energy dependence of isotropic total cross section, $\bar{\sigma}_{1/2\to3/2}$ for $j=\frac{1}{2}\to\frac{3}{2}$ transition summed and averaged over all m_j magnetic sublevels. The arrows along the abscissa indicate the positions of the $j=\frac{3}{2}$ and $j=\frac{1}{2}$ thresholds which are separated by 0.00184 a.u. (1.0 a.u. = 27.211 eV = 2.194×10^5 cm^{-1}). The total energy E is scaled to zero at the non relativistic energy of the F(^2P) atom. Note the abrupt rise in cross section above E = 0.003 which is the height of the repulsive barrier in the $^2\Sigma$ potential.

er solid curve represents the contribution of the $m_j=\frac{3}{2}\to-\frac{3}{2}$ transition to this total. These peak at $l\approx35$, and should be well calculated in terms of the asymptotic potential. The l^{-3} decay of the upper curve is quantitatively predicted by the Born approximation for the long-range R^{-3} ion-quadrupole potential. Although the lower curve transition is forbidden in the Born approximation, it yields a substantial cross section ($187a_0^2$), and as indicated by the l^{-7} falloff, it is in quantitative agreement with a "second-order" version of the Born approximation. These are discussed in Sec. V. The dotted curve in Fig. 1(a) pertains to the total cross section for the $j=\frac{1}{2}$ state, and peaks at $l\approx15$ which is probably too small to allow an asymptotic expansion for the potentials. However, at large l the curve properly decays as l^{-5} as predicted for an R^{-4} ion-induced-dipole potential.

B. Energy Dependence of Cross Sections

The energy dependence of the inelastic $j=\frac{1}{2}\to\frac{3}{2}$ cross section is shown in Fig. 2. In the thermal region, around $E=0.002$ a.u. the cross section is about $0.1a_0^2$. However, above $E=0.003$ a.u., which is approximately the height of the potential barrier in the $^2\Sigma$ potential (see Figs. I-3 and I-4) the cross section increases rapidly, and by $E=0.01$ a.u. $\equiv0.27$ eV, the cross section is $17a_0^2$. Again this is an indication that it is the inner portion of the interaction potentials which play a dominant role in determining the inelastic cross section.

The behavior of the cross section at low energies is complicated by two effects. First, the threshold behavior is aggravated by the R^{-3} long-range potential in the $j=\frac{3}{2}$ channels for which there is no well-defined scattering length. Secondly, the $^2\Sigma$ potential is such that a shape resonance exists owing to tunneling through the potential barrier. This energy region is shown in more detail in the semilog plot of Fig. 3. The structure at $E\approx0.0015$ a.u. is undoubtedly due to the shape resonance in the $^2\Sigma$ potential, but is difficult to assess in any simple way because of the strong three-state couplings. There is, in fact, experimental evidence of such a shape resonance in the photoelectron spectrum of $HF^+(^2\Sigma)$ measured by Berkowitz.[7] The abrupt rise in the cross section at $E=0.003$ a.u. occurs when the barrier is surmounted.

The energy dependence of the $j=\frac{3}{2}$ and $j=\frac{1}{2}$ channel cross sections are shown in Figs. 4 and 5, re-

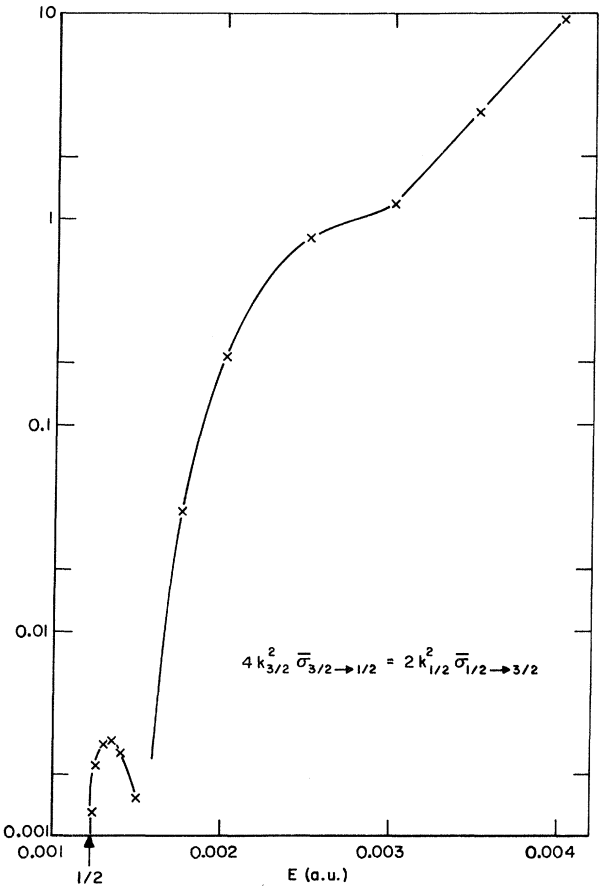

FIG. 3. Semilog plot of $4k^2_{3/2}\bar{\sigma}_{3/2\to1/2}\equiv2k^2_{1/2}\bar{\sigma}_{1/2\to3/2}$ vs total energy E. Threshold for the transition $j=\frac{3}{2}\to\frac{1}{2}$ is indicated by the arrow at $E=0.001\,228$ a.u. The dip at $E=0.0015$ is due in a complicated way to the existence of a shape resonance caused by tunneling through the $^2\Sigma$ potential barrier.

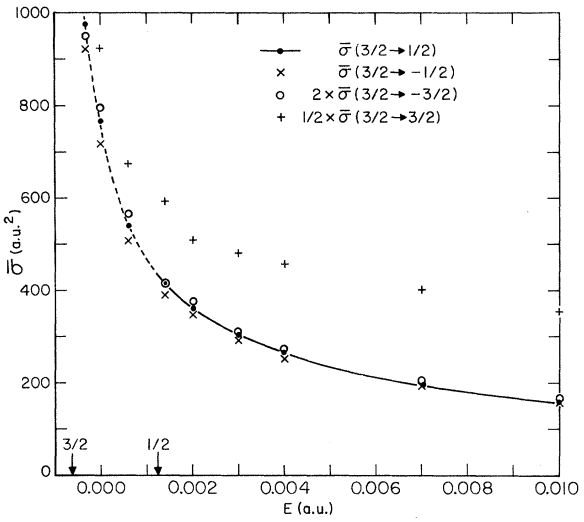

FIG. 4. Energy dependence of the total isotropic cross section $\bar{\sigma}$ for magnetic transitions $m_j \to m_j'$ in the $j=\frac{3}{2}$ state. The curve passes through the data points for the $\frac{3}{2}\to\frac{1}{2}$ transition; the solid portion of the curve is the result of three-state couplings while the dashed portion indicates the energy region when the $j=\frac{1}{2}$ channel is closed and only two-state couplings were considered. The $\frac{3}{2}\to-\frac{1}{2}$ and twice the "forbidden" $\frac{3}{2}\to-\frac{1}{2}$ cross sections fall close to this curve and indicate the constant ratio of these cross sections as a function of energy. The elastic $\frac{3}{2}\to\frac{3}{2}$ transition is also in fairly constant ratio particularly at higher energies.

spectively, and primarily demonstrate the substantial contributions made by the so-called "forbidden" Zeeman transitions. The Zeeman transitions in the $j=\frac{3}{2}$ state determine the magnitude of various depolarization effects which are defined in terms of two cross reactions; a disorientation cross section σ_1:

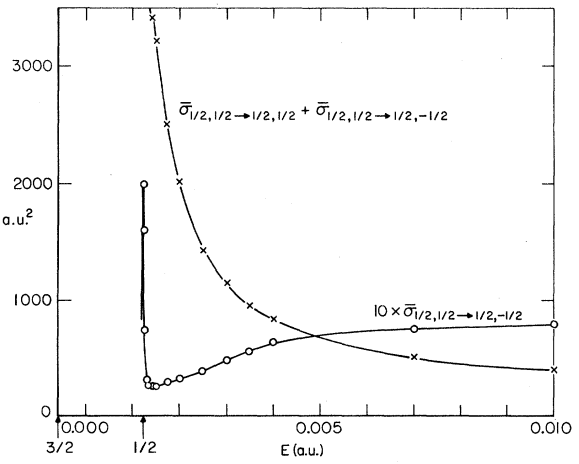

FIG. 5. Energy dependence of the total isotropic cross section $\bar{\sigma}$ for magnetic transitions in the $j=\frac{1}{2}$ state.

$$\sigma_1 = \tfrac{1}{5}\bar{\sigma}_{3/2,1/2\to 3/2,-1/2} + \tfrac{2}{5}\bar{\sigma}_{3/2,3/2\to 3/2,1/2} + \tfrac{8}{5}\bar{\sigma}_{3/2,3/2\to 3/2,-1/2} + \tfrac{9}{5}\bar{\sigma}_{3/2,3/2\to 3/2,-3/2},$$

and a disalignment cross section σ_2:

$$\sigma_2 = 2\bar{\sigma}_{3/2,3/2\to 3/2,1/2} + 2\bar{\sigma}_{3/2,3/2\to 3/2,-1/2}.$$

It can be seen in Fig. 4 that the *ratios* of these cross sections are very insensitive to energy; these ratios are summarized in Fig. 6. σ_1 and σ_2 are then simply related to the cross section for the $(\frac{3}{2}, \frac{3}{2}\to\frac{3}{2}, \frac{1}{2})$ transition

$$\sigma_1 = 2.98\,\bar{\sigma}_{3/2,3/2\to 3/2,1/2}, \quad \sigma_2 = 3.90\,\bar{\sigma}_{3/2,3/2\to 3/2,1/2},$$

and

$$\sigma_2/\sigma_1 = 1.31.$$

The proportionality of σ_1 and σ_2 with respect to the total cross section is less constant with energy, but approximately $\sigma_{3/2,3/2\to 3/2,1/2} \approx 0.15\sigma_{\text{tot}}$. These are to be contrasted, for instance, to the theories of Wang and Tomlinson[8] which predict $\sigma_1 = 2\bar{\sigma}_{3/2,3/2\to 3/2,1/2}$, $\sigma_2 = 4\bar{\sigma}_{3/2,3/2\to 3/2,1/2}$, and $\sigma_2/\sigma_1 = 2$.

V. BORN APPROXIMATION VERSUS EXACT NUMERICAL RESULTS

When the Born approximation[9] is applied to Eq. (2.2) and use is made of the boundary conditions (I-6.3) the following expression for the reactance matrix is obtained:

$$^{B}K^{J}_{j,l;j',l'} = -(k_j k_j')^{1/2}\int_0^\infty dR\, R^2 j_l(k_j R) j_{l'}(k_j' R) \times M^{J}_{j,l;j',l'}(R), \quad (5.1)$$

where

$$M^{J}_{j,l;j',l'} = \frac{2\mu}{\hbar^2}[\delta_{j,j'}\delta_{l,l'}W_1 + C^{J}_{j,l;j',l'}(W_0 - W_1)].$$

Since the transition matrix $\underline{T}$ is related to the reactance matrix, i.e., $\underline{T} = -2i\underline{K}(1-i\underline{K})^{-1}$, an expansion of $\underline{T}$ in powers of $\underline{K}$ yields

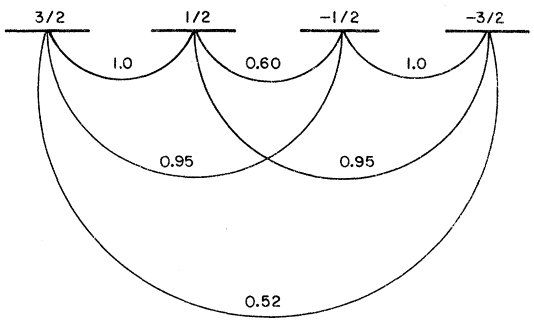

FIG. 6. Relative transition probabilities between the magnetic levels of the $j=\frac{3}{2}$ state normalized to the $\bar{\sigma}_{3/2,3/2\to 3/2,1/2}$ cross section. These ratios are insensitive to energy.

$$\underline{^{B}T} \approx -2i\,\underline{^{B}K} + 2\,\underline{^{B}K}\cdot\underline{^{B}K} + O(\underline{^{B}K}^{3}). \quad (5.2)$$

The leading term is just the usual Born approximation applied to Eq. (2.2) using the $\underline{T}$ matrix boundary conditions of Eq. (I-6.4).

Let

$$D_{j,l;j',l'} = \int_0^\infty dR\, R^2 (k_j k_j')^{1/2} j_l(k_j R) j_{l'}(k_j' R)(2\mu/\hbar^2) \times [\tfrac{1}{3}(2W_1 + W_0)] \quad (5.3)$$

and

$$O_{j,l;j',l'} = \int_0^\infty dR\, R^2 (k_j k_j')^{1/2} j_l(k_j R) j_{l'}(k_j' R)(2\mu/\hbar^2) \times (W_0 - W_1). \quad (5.4)$$

These integrals are easily evaluated if the asymptotic expressions are employed (Eqs. (I-8.7) for the $^2\Pi$ and $^2\Sigma$ HF^+ potentials designated by W_1 and W_0, respectively:

$$\frac{2\mu}{\hbar^2} W_1(R) \sim -\frac{\bar{q}}{R^3} - \frac{\bar{\alpha}}{R^4}, \qquad \frac{2\mu}{\hbar^2} W_0(R) \sim \frac{2\bar{q}}{R^3} - \frac{\bar{\alpha}}{R^4}, \quad (5.5)$$

where $\bar{q}$ = 1078 a.u. and $\bar{\alpha}$ = 7840 a.u.^{2}. The quadrupole term $\bar{q}$ only contributes to $O_{j,l;j',l'}$, while the polarization term $\bar{\alpha}$ only contributes to $D_{j,l;j',l'}$ and, in fact, only influences the diagonal matrix elements of $\underline{^{B}K}$:

$$^{B}K^{J}_{j,l;j',l'} = -\delta_{j,j'}\delta_{l,l'} D_{j,l;j,l} - (C^{J}_{j,l;j',l'} - \tfrac{1}{3}\delta_{j,j'}\delta_{l,l'}) O_{j,l;j',l'}. \quad (5.6)$$

Explicitly these terms are as follows[9]:

$$D_{j,l;j,l} = -\frac{k_j^2 \bar{\alpha}\pi}{(2l+3)(2l+1)(2l-1)}, \quad (5.7)$$

$$O_{j,l;j,l'} = \frac{(\frac{1}{2} + \delta_{l,l'})\, 4 k_j \bar{q}}{(l+l')(l+l'+2)}. \quad (5.8)$$

An expression involving the hypergeometric series $F_{21}(a, b; c; (k_j/k_j')^2)$ is obtained for $j' \neq j$ which rapidly approaches zero for large l and small energies.

Equation (5.1) and (5.2) pertain to the total angular momentum representation $|J, M, j, l\rangle$ and are combined in Eq. (3.3) to yield the matrix $\langle j, m_j, l, m_l | T | j', m_j', l', m_l'\rangle$ which is more directly related to the appropriate cross sections. The Born approximation may be applied directly to the coupled equations in the $|j, m_j, l, m_l\rangle$ representation[5] required in (3.3), and one obtains

$$\langle j, m_j, l, m_l | {}^{B}K | j', m_j', l', m_l'\rangle = -\delta_{j,j'}\delta_{l,l'}\delta_{m_j,m_j'}\delta_{m_l,m_l'} D_{j,l;j',l'} + (j', j, 2 | m_j', -m_j, m_j' - m_j) \times (2, l, l' | m_j - m_j', m_l, m_l')(2, l, l' | 0, 0, 0)\left(\frac{2l+1}{2l'+1}\right)^{1/2} (-1)^{m_j - m_j'} \left(\frac{2}{3}\right) O_{j,l;j',l'}. \quad (5.9)$$

Certain selection rules are obtained from the Clebsch-Gordan coefficient $(j', j, 2 | m_j', -m_j, m_j' - m_j)$ in Eq. (5.9). It is found that the first-order transition matrix $\underline{^{B}T} \approx -2i\,\underline{^{B}K}$, and hence the cross sections, vanish for the following transitions.

$$^{B}\sigma_{j,m_j \to j,-m_j} = 0. \quad (5.10)$$

This result applies to both $\bar{\sigma}$ and σ^0, and says that in the Born approximation a change in the *sign* of the magnetic quantum number m_j is forbidden. Note that all such transitions tabulated in Table II decay as l^{-7} and are consistent with this rule, *to first order in* $\underline{^{B}K}$.

As indicated in Eq. (5.2) terms in $\underline{^{B}K}\cdot\underline{^{B}K}$ may also contribute to the cross sections. Although such terms predict the quantitatively observed (k^2/l^7) dependences of the "forbidden" transitions, in fact, they do *not* contribute to these particular transitions. It is possible to develop a second Born approximation to the reaction matrix K, but unfortunately the necessary integrals cannot be evaluated analytically. However, various approximations may be applied to the expression, and each predicts the (k^2/l^7) dependence and the proper magnitude for the transitions in Eq. (5.10).

The numerical results for the "allowed" transitions are in quantitative agreement with (5.6) and (5.9), and the functional dependence of these cross sections on l, for large l, can be utilized to correct the numerical results for contributions from $l = l^*$ to ∞, as expressed in Eq. (3.4) and Table II.

For instance, the sum, for $m_j \neq m_j'$, in Eq. (3.1) yields

$$\sum_{l',M} \mathcal{G}_{l,l',M}\mathcal{G}^*_{l',l',M} = (j, j, 2 | m_j', -m_j, m_j' - m_j)^2 \times k_j^2 \bar{q}^2 \frac{16(2l+1)}{15(2l+3)(2l-1)l(l+1)}\left(1 + \frac{5}{4(l-1)(l+2)}\right) \underset{l\to\infty}{\sim} (j, j, 2 | m_j', -m_j, m_j' - m_j)^2 \times k_j^2 \bar{q}^2 \frac{8}{15 l^5}. \quad (5.11)$$

The ratio of the calculated and Born cross sections is shown in Fig. 7. As a function of increasing l the ratio for $(\frac{3}{2}, \frac{3}{2} \to \frac{3}{2}, \frac{1}{2})$ rapidly approaches 1 to within 1% for both $E = 0.002$ and $E = 0.01$ a.u. The elastic cross section, with $j = j' = \frac{3}{2}$, $m_j = m_j'$ is

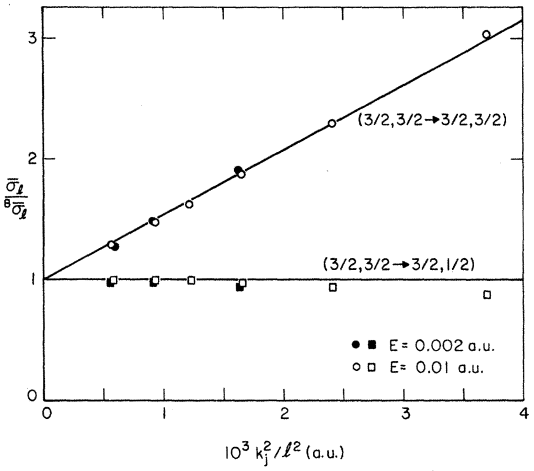

FIG. 7. Ratio of the calculated isotropic total cross sections $\bar{\sigma}_l$ to the first-order Born approximation prediction ${}^B\bar{\sigma}_l$ for magnetic transitions in the $j=\frac{3}{2}$ state as a function of partial wave l. As $k_j^2/l^2 \to 0$ these ratios approach 1 indicating the validity of the Born approximation for large l. These dependences are summarized in Table II. The deviation of the elastic $(\frac{3}{2}, \frac{3}{2} \to \frac{3}{2}, \frac{3}{2})$ cross section is expected and is quantitatively due to contributions from the polarization potential which was not included in ${}^B\bar{\sigma}_l$.

a bit more complicated due to contributions from both the $D_{l,l';j,l}$ and the $O_{l,l';j,l}$ terms in Eq. (5.9), but in the limit, as $l \sim \infty$, the second term will dominate and the asymptotic cross section is given by (5.11). This behavior is demonstrated in Fig. 7 for $\bar{\sigma}(\frac{3}{2}, \frac{3}{2} \to \frac{3}{2}, \frac{3}{2})$ which extrapolates to the Born result to within about 5%.

The elastic term in the $j=j'=\frac{1}{2}$ state $(m_j=m_j')$ sums to the observed $\bar{\sigma}(k^2/l^5)$ dependence of the numerical cross sections,

$$\sum_{l',M} \mathcal{G}_{l,l',M}\mathcal{G}^*_{l,l',M}(j=j'=\tfrac{1}{2},\ m_j=m_j') = k_j^4 \frac{\bar{\alpha}^2\pi^2 4}{(2l+3)^2(2l+1)(2l-1)^2} \underset{l\to\infty}{\sim} k_j^4 \frac{\bar{\alpha}^2\pi^2 4}{32 l^5}. \quad (5.12)$$

This is demonstrated in Fig. 8.

Similar quantitative agreement is obtained from the zero-angle cross sections. The interference terms in Eq. (3.2) lead to an additional first-order Born selection rule for σ^0 which is consistent with Table II:

$${}^B\sigma^0_{3/2,m_j\to 3/2,m_j\pm 1} = 0. \quad (5.13)$$

The calculated k^2/l^7 dependence of all the "forbidden" transitions is demonstrated by the $\bar{\sigma}_l(\frac{3}{2}, \frac{3}{2} \to \frac{3}{2}, -\frac{3}{2})$ cross section which is plotted in Fig. 8.

VI. CONCLUSIONS

The H^+ plus $F(^2P_{j,m_j})$ system has many simplifying features[1] which makes it amenable to a relatively rigorous calculation of the fine-structure transitions $(j,\ m_j \to j',\ m_j')$. However, many of the resultant conclusions concerning these cross sections should be of general validity. This is particularly true for systems with a fine-structure splitting comparable to the 404-cm^{-1} splitting in $F(^2P)$.

A. Inelastic $j \to j'$ Transitions

The $(\frac{3}{2},\ m_j \to \frac{1}{2},\ m_j')$ transition only occurs for small partial waves and is determined by the potential characteristics at small (3-a.u.) to intermediate (10-a.u.) interatomic distances. For such small partial waves ($l = 0 - 20$) a close-coupling calculation is required (three channels for a $^1S + {}^2P$ system) in order to obtain accurate partial cross sections. There is a negligible contribution to the total cross section from larger l waves where the Born approximation or even the two-state distorted-wave approximate would apply. These conclusions are contingent on a moderately large splitting which requires a close-in collision in order to induce transitions. The role of close-coupling effects in systems with small splittings remains to be assessed. A study of $He + Na(^2P)$ is being undertaken for this purpose.

B. Magnetic $m_j \to m_j'$ Transitions

1. $j = \frac{1}{2}$ state

The conclusion arrived at concerning the importance of close-in strong-coupling collisions in determining the inelastic $j = \frac{3}{2} \to \frac{1}{2}$ transition also applies to the $m_j = \frac{1}{2} \to -\frac{1}{2}$ transition in the $j = \frac{1}{2}$ state.

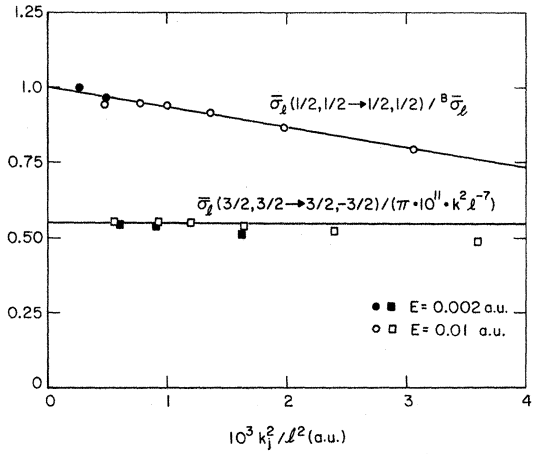

FIG. 8. The l^{-5} dependence of the elastic $\bar{\sigma}_l(\frac{1}{2}, \frac{1}{2} \to \frac{1}{2}, \frac{1}{2})$ cross section is quantitatively explained by the first-Born approximation since the ratio $\bar{\sigma}_l/{}^B\bar{\sigma}_l$ approaches unity as $(k_j^2/l^2) \to 0$. Those transitions, such as $\bar{\sigma}_l(\frac{3}{2}, \frac{3}{2} \to \frac{3}{2}, -\frac{3}{2})$, which are "forbidden" by the first-order Born approximation, all vary as (k^2/l^7). This can be attributed to the contributions of the second-order Born approximation. The magnitude of $\bar{\sigma}_l(\frac{3}{2}, \frac{3}{2} \to \frac{3}{2}, -\frac{3}{2})$ at large l is predicted to within a factor 2 to 3 by various approximate solutions to the second-order Born approximation.

This transition requires an intermediate coupling to the $j=\frac{3}{2}$ channels during the collision, and although the cross section is from 100 to 5 times larger than the $j=\frac{1}{2}\rightarrow\frac{3}{2}$ cross section, it only occurs in association with the inelastic partial waves [see Fig. 1(b)].

The cross section $(\frac{1}{2},\ \frac{1}{2}\rightarrow\frac{1}{2},\ -\frac{1}{2})$ increases with energy from $30a_0^2$ at $E=0.002$ a.u., where it is 10 times smaller than the $\frac{1}{2}\rightarrow-\frac{1}{2}$ magnetic transition in the $j=\frac{3}{2}$ state, to $80a_0^2$ at $E=0.01$ where it is comparable to the decreasing $j=\frac{3}{2}$ transition. Indeed this transition has the smallest cross section of those that are predicted to be zero in the Born approximation, but it is by no means "forbidden". The effect of a decreased spin-orbit splitting on the $(\frac{1}{2},\ \frac{1}{2}\rightarrow\frac{1}{2},\ -\frac{1}{2})$ transition is difficult to predict at this time.

2. $j=\frac{3}{2}$ state

The "forbidden" $m_j\rightarrow -m_j$ transitions in the $j=\frac{3}{2}$ state are at most only a factor of 2 smaller than the "allowed" magnetic transitions. Their cross sections decrease with energy and are in approximate constant ratio (~1 : 5) to the elastic cross sections (see Figs. 4 and 5, Table I). The second-order Born approximation makes contributions to *both* the off-diagonal $K^J_{3/2,l;3/2,l\pm2}$ *and* the diagonal $K^J_{3/2,l;3/2,l}$ reactance matrix which can give rise to these transitions. No coupling to the $j=\frac{1}{2}$ channel is required and the general breakdown of the $m_j\not\rightarrow -m_j$ prediction in the $j=\frac{3}{2}$ state should be independent of the splitting. It is unlikely that this violation is specific to $H^+ + F(^2P)$ and one must conclude that such transitions generally occur.

The $m_j=\frac{3}{2}\rightarrow\frac{1}{2}$ transition in σ^0 which is also forbidden in the Born approximation, is significantly smaller than the $m_j\rightarrow -m_j$ transition. This is explicable in terms of coupling to a single intermediate state in the $|j,\ m_j,\ l,\ m_l\rangle$ representation which can lead to the $m_j\rightarrow -m_j$ transition but not to $m_j=\frac{3}{2}\rightarrow\frac{1}{2}$. Note, however, that this is strictly an artifact of the interference terms that occur in Eq. (3.2) for an incident beam parallel to the axis of quantization. The comparable cross section for $\bar{\sigma}$, which is an average over an isotropic distribution of incident angles, is "allowed" even in the first-order Born approximation. This is a general phenomenon with spatially degenerate transitions, and one should exercise great caution in inferring gas-phase rate constants for magnetic transitions from a beam experiment. The lack of detailed balance in the σ^0 cross sections is expected theoretically. The significant cross sections for application to gas-phase statistical theory are the isotropic cross sections $\bar{\sigma}$ which are *directly* convertible to rate constants and which do obey detailed balance.

C. Molecular Theory

For large partial waves the agreement of the Born approximation with the exact molecular-theory results indicates that an expansion in an atomic basis, which would equally well represent the dominant, long-range R^{-3} quadrupole interaction, is adequate to determine the off-diagonal transition matrix. However for small partial waves, which solely determine the inelastic $j=\frac{1}{2}\rightarrow\frac{3}{2}$ transition, at least for splittings in the range of 404 cm^{-1}, the interaction energy is no longer dominated by the R^{-3} quadrupole interaction, or even the R^{-4} polarization potential. An atomic basis is useless since it would require an infinitude of excited atomic closed-channel states to represent the $^2\Pi$ and $^2\Sigma$ electronic wave functions which already properly incorporate the effects of polarization, exchange, and chemical binding (e.g., charge transfer) within an adiabatic, or perturbed-stationary-state, approximation.

The importance of the molecular states also implies that the R dependence of the molecular spin-orbit matrix elements must be determined, and one cannot generally use the asymptotic atomic matrix elements. In addition, it may be necessary to evaluate the BO breakdown terms arising from the nuclear kinetic-energy operation, and in particular, the nuclear orbital angular momentum operation (Λ-doubling terms). Fortunately, both these effects can be estimated and are found to be negligible[1] for $H^+ + F$. *However the conclusion applies to* HF^+ *only*! It is expected that for systems other than HF^+ the R dependence of these terms may substantially influence the couplings. Without a knowledge of these coupling matrix elements the accurate molecular potentials that are becoming increasingly available are of insufficient use by themselves to perform quantitative scattering calculations.

ACKNOWLEDGMENTS

The author is grateful to Dr. A. C. Wahl and Dr. M. Krauss for the molecular calculations of HF^+ that were provided for this study, and to Professor L. Krause for his stimulating discussions.

---

[1] F. H. Mies, preceding paper, Phys. Rev. A 7, 942 (1973). This will be referred to as Paper I, and corresponding equations, etc., will be denoted by this prefix, e.g., Eq. (I-7.1), Fig. (I-1), Table (I-1).

[2] R. Gordon, J. Chem. Phys. **51**, 14 (1969).

[3] R. Gordon, Methods Comput. Phys. **10**, 81 (1971).

[4] W. A. Lester, Jr. and R. B. Bernstein, Chem. Phys. Lett. **1**, 207 (1967); Chem. Phys. Lett. **1**, 347 (1967).

[5] $\mathcal{G}_{l,l',M}$ is the T matrix for the equivalent channel representation $|j,\ m_j,\ l,\ m_l\rangle = Y_l m_l(\hat{R})\,|\vec{R},\ j,\ m_j\rangle$, where the total angular momen-

tum states J, M are not isolated in the close-coupling expansion.

[6]The strong-coupling region is recognized by the presence of interference terms which cause the cross sections in Fig. 1(a) to behave erratically with l and by the close proximity of these curves to the dashed curve which represents the upper bound where $\underline{T} = 2 \times \underline{1}$.

[7]J. Berkowitz, Chem. Phys. Lett. **11,** 21 (1971).
[8]C. H. Wang and W. J. Tomlinson, Phys. Rev. **181,** 115 (1969).
[9]N. F. Mott, and H. S. W. Massey, *The Theory of Atomic Collisions* (Oxford U. P., Oxford, England, 1965).

PHYSICAL REVIEW A VOLUME 7, NUMBER 3 MARCH 1973

Measurement of the Lifetime and the Electron-Impact Excitation Cross Section and Polarization of the 2^3P Term of Singly Ionized Lithium*

A. Adler,† W. Kahan,‡ and R. Novick
Columbia Radiation Laboratory, Columbia University, New York, New York 10027

T. Lucatorto
Columbia Radiation Laboratory, New York, New York 10027
and National Bureau of Standards, Washington, D. C. 20234§

(Received 4 October 1972)

The lifetime of the $2\ ^3P_j$ states in singly ionized lithium has been measured using an rf magnetic-resonance technique; the value is $\tau = 45 \pm 5$ nsec. Neutral lithium was ionized and excited by a unidirectional beam of electrons which produced an alignment in the excited state. The cross section for the electron-impact excitation $1s^2\ 2s\ ^2S \rightarrow 1s2p\ ^3P$ near threshold was measured to be $10^{-22\pm1}$ cm^2. Implications for the feasibility of rf resonance spectroscopy on the fine and hyperfine structure of the $2\ ^3P$ term will be discussed.

I. INTRODUCTION

An accurate measurement of the fine and hyperfine structure of Li^+ would be a very important addition to atomic spectroscopy. Two-electron atomic systems are of considerable theoretical interest because their relative simplicity allows very accurate calculations. In particular, comparisons of fine- and hyperfine-structure calculations for such systems with precision measurements of these quantities have provided a critical test of quantum electrodynamics and, until the recent transfer to the use of the ac Josephson-effect measurements, the accepted value for the electromagnetic coupling constant, $\alpha = e^2/hc$.

Probably the most intensively studied two-electron system has been that of the 2^3P multiplet in He. Hughes and his collaborators have used an atomic-beam double-resonance technique to measure the fine-structure splittings to ~ 1 ppm.[1] Recently, new theoretical values for the splittings have been obtained which give the 2^3P_0-2^3P_1 separation to ~ 6 ppm and the 2^3P_1-2^3P_2 separation to ~ 150 ppm.[2] The new level of accuracy achieved in this calculation is derived mainly from a preliminary evaluation of newly developed $\alpha^6 mc^2$ terms for the two-electron Hamiltonian, and an eventual accuracy of better than 1 ppm is expected from the continued refinement of this approach. Thus, there is the expectation that the He fine structure will provide a value for α better than 1 ppm.

Some of the reasons which make the intensive study of the 2^3P term in He so valuable also apply in the case of Li^+. The fact that the ratio of natural linewidth to fine-structure splitting in the 2^3P Li^+ term is about 1.2×10^{-4} means that a 1 ppm accuracy in the fine-structure measurement can be achieved by measuring the center of the resonance line to only $\frac{1}{100}$ of its width. Wave functions for this term in Li^+ have already been calculated to about the same accuracy as the He functions and have been used to provide the fine-structure splittings to order α^4 Ry.[3] The lithium study has two additional features.

(a) The fine structure of Li^+ is predominantly due to the spin-spin term; this fact means that the results in Li^+ can provide a more sensitive test for the correctness of the two-electron, spin-spin Hamiltonian than those in He, where the spin-orbit and spin-spin terms contribute about equally.

(b) In the course of the measurements the Li^+ hyperfine structure must also be determined to 2 parts in 10^5; the comparisons between experiment and the hfs calculations can advance our understanding of nuclear structure effects in hfs.

Our work on singly ionized lithium was initiated with the hope of eventually measuring the fine structure of the 2^3P term. Figure 1 is an energy-level diagram showing the fine and hyperfine structure of $^7Li^+$. rf or microwave resonance spectroscopy of the 2^3P states can be performed if the system is prepared having some alignment. Of the